scientific reports

Check for updates

OPEN

Air-coupled piezoelectric micromachined ultrasonic transducer array based on low-cost and large remnant polarization PZT thin film

Jia-Ling Lin[1], Ya-Han Liu[2], Chien-Lun Kao[1], Shao-Wei Wu[1], Han-Jen Hsu[1], Hsiao-Chi Lin[1], Chih-Ying Li[1], Chun-Yuan Chen[1], Yeong-Her Wang[2]✉ & Chih-Hsien Huang[1]✉

Due to the development of semiconductor technology, control and driving circuits for large phased arrays have become cheaper and more compact, enabling air-coupled ultrasonic transducer arrays to be applied in areas such as ultrasonic haptic feedback and acoustic levitation. However, current air-coupled ultrasonic transducers are quite bulky, which prevents the commercialization of these applications. Hence, piezoelectric micromachining ultrasonic transducers (pMUT) have been proposed to replace conventional ultrasound transducers. Currently, PZT, or lead zirconate titanate, thin film is the most reliable and, consequently, most popular piezoelectric layer for pMUT, but existing PZT fabrication methods are too expensive or require rare metals. To counter this problem, this study proposed a cost-effective and reliable PZT thin film fabrication method. By depositing a commercial sol-gel solution as a seed layer followed by radio frequency sputtering, a PZT thin film with remnant polarization of 113.35 μC/cm^2 and a coercive field of 211.6 kV/cm was demonstrated. Moreover, high-throughput air-coupled pMUTs and pMUT arrays were made based on the proposed PZT thin film. Finite element method simulations were conducted to optimize the structure parameters for the 40 kHz pMUT. A standard microphone was used to measure the acoustic pressure at 3 cm above the pMUT and the pMUT array to evaluate their performance. The pMUT generated an acoustic pressure of 0.764 Pa/V with a resonance frequency of 52.2 kHz, and the pMUT array's maximum acoustic pressure was 87.4 Pa. The device demonstrated the highest acoustic output pressure among existing sub-100 kHz air-coupled pMUT arrays using PZT as the actuation layer, highlighting the potential of using the proposed PZT thin film deposition method for high-pressure mid-air ultrasonic applications.

Keywords Acoustic levitation, Non-contact, Tweezer, Acoustic trap, Transducer array

Micromachined ultrasonic transducers were first demonstrated in the 1970s[1]. More specifically, the piezoelectric micromachining ultrasonic transducers (pMUT) have been discussed frequently due to low energy consumption, high bandwidth, and low DC bias voltage requirement. They have been widely used in non-destructive testing, fingerprint recognition, and medical imaging[2–5]. Recently, pMUTs have demonstrated the potential in high-pressure ultrasound applications in the air, such as range detection and ultrasonic haptic feedback[6,7]. These applications open opportunities for contactless interfaces, mid-air interactions, and advanced sensing technologies, making pMUTs a promising solution for human-machine interfaces in the next generation. A pMUT consists of a piezoelectric layer, an elastic layer, a top electrode, and a bottom electrode. When an electrical field is applied to the piezoelectric layer, the piezoelectric effect introduces lateral strain and deforms the layer[8]. The deformation vibrates the elastic layer as well as the medium. If the applied electric field alternates at a frequency in the range of ultrasonics, the vibration of the pMUT would generate ultrasound signals in the medium. As the source of the mechanical deformation, the material of the piezoelectric layer is essential for the efficiency of the pMUTs, and $Pb[Zr_xTi_{1-x}]O_3$ (PZT), ZnO, AlScN, and PVDF are currently commonly used for

[1]Department of Electrical Engineering, National Cheng-Kung University, Tainan, Taiwan. [2]Institute of Microelectronics, National Cheng-Kung University, Tainan, Taiwan. ✉email: yhw@ee.ncku.edu.tw; chihhsien_h@mail.ncku.edu.tw

that purpose[9,10]. Among these, PZT is the most popular material since its piezoelectric coefficient is an order of magnitude higher than the others. Therefore, pMUTs based on PZT usually have better electromechanical coupling, making them a top choice for high-throughput ultrasonic applications. However, a reliable and cost-effective PZT thin film deposition method has been an ongoing quest.

To improve the quality of PZT thin films, researchers have worked on optimizing the fabrication process for decades, including the material of the bottom electrode/seed layer, annealing/deposition parameters, and the ratio of zirconium and titanium[11–13]. The optimizations of the bottom electrode and seed layer remain a challenge. Generally, PZT thin films are polarized through a high-temperature annealing process to convert the crystal lattice from pyrochlore to perovskite. However, high annealing temperatures might induce cracks in the film due to a thermal expansion mismatch between the film and the substrate[14]. This issue directly affects the reliability and efficiency of PZT fabrication, limiting their use in mass production and wider applications. To alleviate this situation, a buffer layer with a similar thermal expansion coefficient and lattice constant as PZT is deposited on the substrate before growing the thin film. This buffer layer can be an extra seed layer or a bottom electrode. For instance, conductive metal oxides like $SrRuO_3$ (SRO) and $LaNiO_3$ (LNO) can be deposited as the seed layer to enhance crystallization uniformity[15,16]. These metal oxide layers are typically deposited by sputtering or spin coating, followed by thermal annealing[16]. On the other hand, Pt is usually used as the bottom electrode for depositing PZT thin films with Ti as an adhesion layer[17]. Some studies have used both the seed layer and bottom electrode for further improvement[18]. Besides, doping the PZT target with Nb and Mn increases the piezoelectric constant and reduces the dielectric constant of the sputtered thin film, respectively, improving the efficiency and sensitivity of the deposited PZT thin film[19,20].

Although these methods have demonstrated convincing results in improving the properties of PZT thin film, the deposition of conductive metal oxide and doping of the PZT target with rare metals either require specific equipment and an additional annealing process or increase the cost dramatically. Moreover, the recipes for depositing conductive metal oxide are diverse depending on the equipment and are hard to reproduc[21,22]. To overcome these limitations, it is critical to develop an economical and efficient manufacturing method that maintains high piezoelectric performance without compromising reliability. These reliability and cost issues have prevented them from being used in the mass production of pMUTs. To solve these issues, this study proposed a cost-effective and reliable PZT thin film deposition method for fabricating pMUTs. It utilized a commercial sol-gel PZT as a seed layer, on which the main PZT thin film was grown epitaxially by radio frequency (RF) sputtering. The study analyzed the crystallization and electrical properties of the PZT thin film, as well as its piezoelectric coefficient. Then, pMUTs and pMUT arrays operating at 40–60 kHz were designed and fabricated to verify the performance through the amplitudes of the output acoustic pressures. Finally, the piezoelectric performance and acoustic pressure output of the proposed pMUTs are evaluated and demonstrated for mid-air ultrasonic applications, emphasizing their significance in practical use and technological innovation.

The rest of this article is organized as follows. *Methods* introduce the design and fabrication process of PZT thin film and pMUT. *Result and discussion* demonstrate the characterization results of the PZT thin film and the pMUT, including the remanent polarization value and the piezoelectric coefficient. The output results of the pMUT array are also presented. *Conclusion* summarizes the results of this study.

Methods

Fabrication and characterization of the PZT thin film

As mentioned in *introduction*, Pt has excellent thermal stability and a lattice constant similar to that of PZT. Hence, an electron beam evaporator was used to deposit a 20 nm Ti on the Si substrate as the adhesion layer, followed by a 250 nm Pt layer. In general, sputtering a few micrometers of PZT thin film in a low-pressure chamber produces better uniformity, less contamination, and consumes less labor force than films prepared by preparing films with the sol-gel method. However, optimizing the deposition conditions that allow the PZT thin film to survive rapid thermal annealing over 600 °C without cracking is time-consuming, especially for general RF sputter equipment not customized for depositing PZT. Fortunately, reliable sol-gel PZT precursors have been commercialized recently and can help with this issue. However, it is expensive to grow a micrometer-thick PZT thin film with commercial sol-gel PZT precursors. Therefore, this research used a commercial sol-gel PZT precursor as a seed layer to reduce the thermal lattice mismatch between the sputtered PZT and the bottom electrode, consuming much less of the expensive sol-gel solution. Consequently, the cost could be reduced while securing the reliability of the PZT thin film.

The detailed fabrication process is shown in Fig. 1. Firstly, a 100 nm PZT seed layer was deposited on a prepared substrate by spin-coating a commercial metal oxide (10% PZT-E1 solution [110/52/48], Mitsubishi Materials)[23]. The solution was applied to the substrate spinning at 1000 rpm for 10 s and then at 3000 rpm for 60 s. Next, the solution was dried on a 300 °C hotplate for 5 min to evaporate the organic solvent and form a film. This spin coating process was repeated two more times, and the film was annealed in oxygen at 650 °C using rapid thermal annealing (RTA) in oxygen for 1 min. After the seed layer was produced, another layer of PZT film was deposited by RF sputtering using a $PbTi_{0.48}Zr_{0.52}O_3$ ceramic target under the conditions listed in Table 1[23]. The deposition rate was tested at RF powers ranging from 250 W to 450 W. Finally, the deposited PZT thin films were annealed in oxygen using RTA. Since the proportion of the perovskite crystal lattice and the chance of cracks both increase with the annealing temperature, this study tested several RTA temperatures to find the most reliable conditions for making the pMUTs: 600 °C, 650 °C, and 700 °C with a gradient of 30 °C/s for 180–300 s.

To verify the efficacy of the proposed method, an RF-sputtering PZT thin film without a seed layer was also fabricated in this study for comparison. Since the perovskite phase was an indicator of the piezoelectric properties of PZT, an X-ray diffractometer (XRD, Bruker D8 Discover) was used to inspect the crystal orientation and

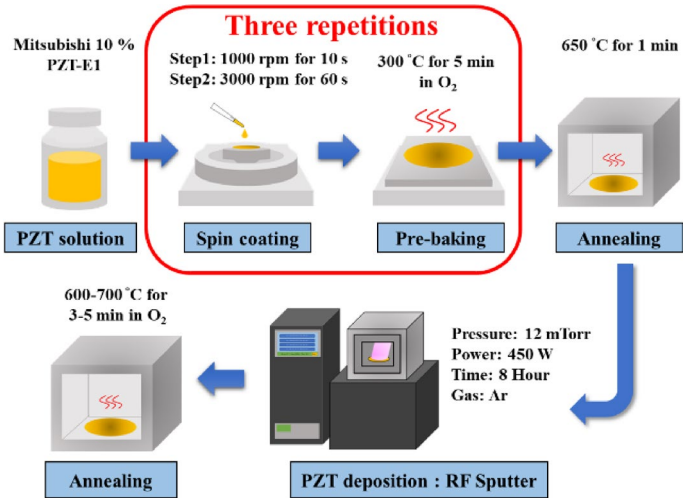

Fig. 1. Proposed PZT thin film deposition process[23].

Parameter	Value
Substrate	Sol-gel PZT/Pt/Ti/Si
Substrate-target distance (cm)	15
Substrate temperature (oC)	25
Target	$PbTi_{0.48}Zr_{0.52}O_3$
Base pressure (mTorr)	5×10^{-6}
Sputtering pressure (mTorr)	12
Sputtering gas	Ar
Deposition power (W)	250–450
Deposition time (hour)	7–10

Table 1. Deposition conditions for RF sputtering[23].

analyze the relative peak intensities. Besides, a film thickness profiler (α-step) was used to check the thickness and uniformity of the films. Moreover, a focused ion beam system (FIB) punctured the pMUT in several locations to observe the cross-sections using scanning electron microscopy. As for the ferroelectricity of the PZT thin film, the polarization-electric field hysteresis loop (P-E loop) and its corresponding capacitance were measured by a ferroelectric analyzer (Precision LC II). The remanent polarization value (P_r) was obtained from the P-E curve to indicate the amount of polarization (charges per area) that remained in the material without an electric field. After that, the transverse piezoelectric constant d_{31} was calculated from the P_r using

$$d_{31} = 2Q_{12}P_r\epsilon_r\epsilon_0, \tag{1}$$

where Q_{12} is the electrostriction coefficient of the PZT thin film, and ϵ_r and ϵ_0 are the relative permittivity (dielectric constant) and the vacuum permittivity of PZT, respectively[22,24]. This study used a Q_{12} value of -3.1 $\times 10^{-2}$ m^4/C^2 based on previous research[25,26]. Since the vibration of pMUT's membrane came from the lateral strain of the piezoelectric layer, the effective deformation of the proposed PZT film was perpendicular to the applied electric field. Hence, the transverse piezoelectric constant d_{31} was an indicator of the efficiency of the pMUT.

Design and modeling of PMUTs

The efficiency of the pMUT was not only defined by the properties of the piezoelectric layer but also influenced by the design of the structure. This study built a model for pMUT and another for the pMUT array before fabrication to predict the pMUT's performance. First, the finite element method (FEM) was used to model a single pMUT using COMSOL Multiphysics 5.6 (COMSOL, Inc.). The FEM model was built using the two-dimensional axisymmetric approach to improve computational efficiency. As shown in Fig. 2a, the stack structure of the circular device consisted of a piezoelectric layer, two substrate layers, and two electrode layers. According to a previous study, the ratio between the radius of the active region and the membrane was designed to be approximately 66% to achieve the maximum vibration of a pMUT, as shown in Fig. 2b[27].

This study aimed to demonstrate a high-efficiency pMUT for mid-air applications. The most commonly used resonance frequency of transducers for mid-air ultrasonic applications is 40 kHz[28]. Therefore, the thickness of each layer was kept constant in the beginning to find the membrane radius that had a resonance frequency of

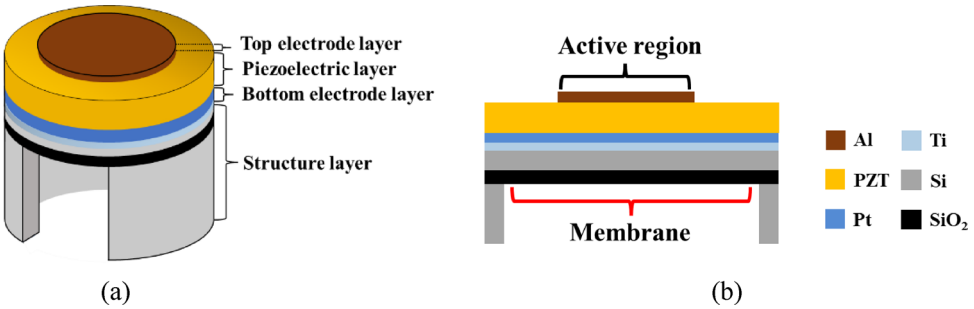

Fig. 2. (**a**) Structure of the proposed pMUT. (**b**) Side view of the FEM model of the proposed pMUT.

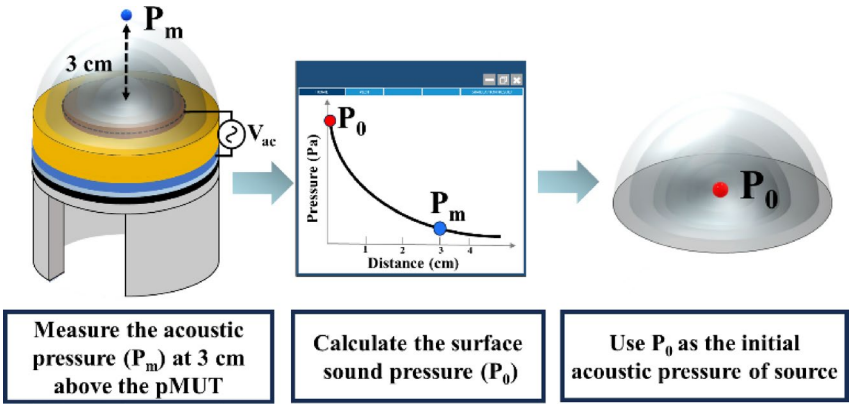

Fig. 3. Method for simulating pMUT array by replacing the single pMUT with an acoustic source. P_m is the acoustic pressure measured at 3 cm above the pMUT. P_0 is the initial acoustic pressure of the emitting source, which is calculated from P_m.

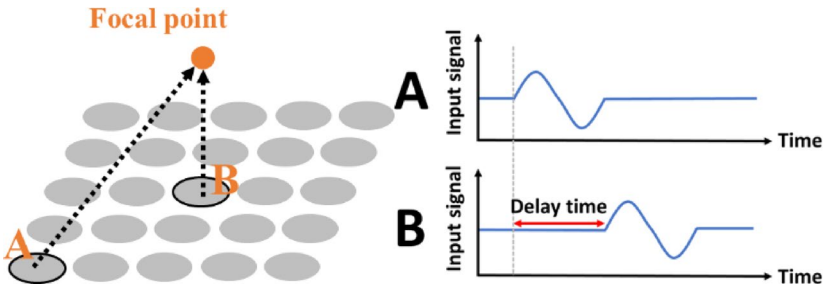

Fig. 4. Acoustic beamforming of a pMUT array. The pMUTs were replaced by planar acoustic sources.

40 kHz. After that, the thickness of the piezoelectric layer was examined to find the displacements of the center of the membrane.

This simulation modeled the pMUT as a planar acoustic source emitting an acoustic burst with a magnitude equal to the surface acoustic pressure of the pMUT. As Fig. 3 presents, since the surface sound pressure was impossible to measure, this study measured the acoustic pressure 3 cm above the pMUT. Then, k-Wave was used to find the surface acoustic pressures corresponding to the two closest simulated acoustic pressures with the same height. Next, interpolation was applied to them to identify the amplitude of the pMUT's initial acoustic burst. In the simulation, the transducer array was built in a $250 \times 250 \times 250$ grid space with a grid size of 250 µm. This array was centered on the X-Y plane, where the number, dimension, and pitch of the pMUT were adjustable. As Fig. 4 illustrates, a focal spot can be assigned if necessary, and the phase delay of each pMUT can be calculated based on the distance between the focal point and the pMUT. The accuracy of the k-Wave model can be verified by measuring the fabricated pMUT array.

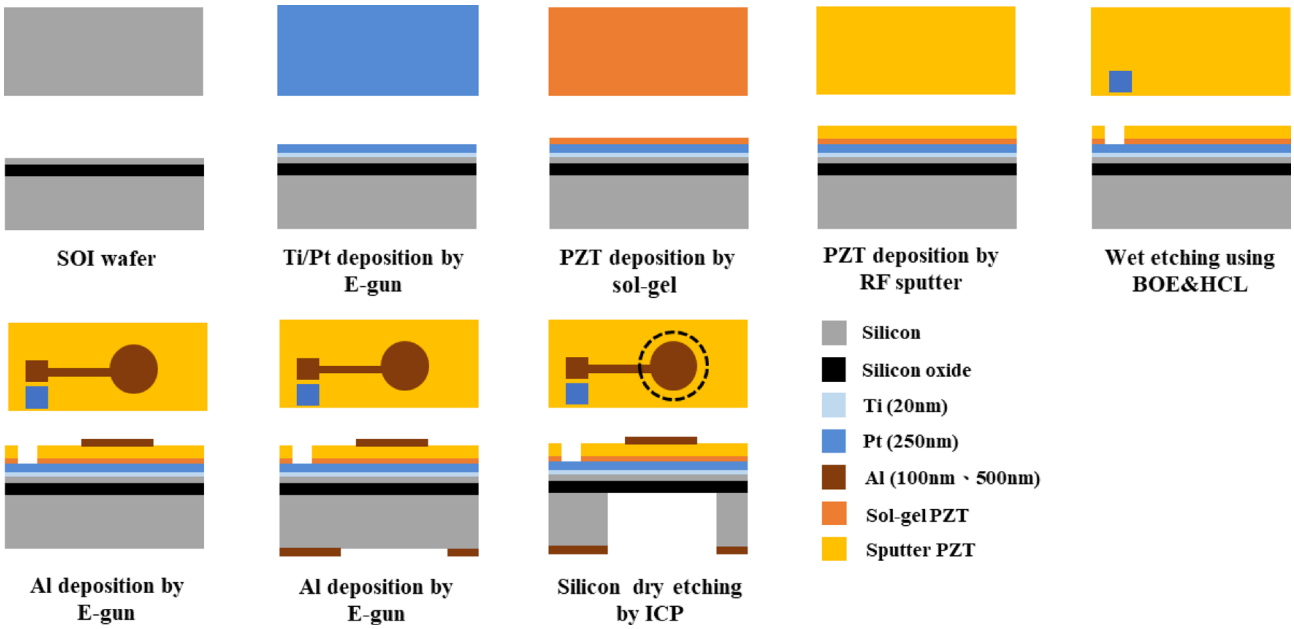

Fig. 5. Fabrication procedure of the pMUT. *SOI* silicon-on-insulator, *BOE* buffered oxide etch, *ICP* inductively coupled plasma.

Parameter	Value (μm)
Thickness of the top electrode (Al)	0.1
Thickness of the sol-gel PZT	0.1
Thickness of the sputter PZT	1.4
Thickness of the bottom electrode (Ti/Pt)	0.02/0.25
Thickness of the substrate	375
Radius of the cavity and the bottom electrode	600–725 (with a deviation of 25 μm)
Radius of the top Al electrode	0.67 × Radius of the cavity

Table 2. Structural parameters of the proposed pMUTs[23].

Fabrication and characterization of pMUTs and pMUTs array

We fabricated pMUTs with actuation layers using the proposed PZT thin film deposition method to verify its performance and reliability. Figure 5 shows the fabrication procedure. Firstly, a commercial silicon-on-insulator wafer with a silicon device layer thickness of 5 μm and a buried SiO_2 layer of 1 μm was used as substrate. Ti (20 nm) and Pt (250 nm) were then deposited as the bottom electrode via electron-beam evaporation. After that, a PZT thin film was deposited using the proposed method as the actuation layer of the pMUT. Since the PZT layer was on top of the bottom electrode, it had to be removed to release the bottom electrode. Therefore, the wafer was patterned with a photoresist (s1813), followed by etching the PZT thin film with buffered oxide etch (HF: NH_4F = 1:6) for 8 min. Subsequently, the wafer was soaked in HCl for 1 min to remove any residues[29]. Afterward, the Al top electrode was deposited and patterned via the electron-beam evaporation and lift-off process. Then, Al with a thickness of 500 nm was deposited and patterned on the backside of the wafer as the etching mask. Finally, the cavities were formed by a deep etching process using inductively coupled plasma etching. The detailed fabrication parameters of the pMUT are listed in Table 2[23].

After fabricating the pMUTs and pMUT arrays, a series of measurements were performed to analyze their properties. First, the depth, radius, and verticalness of a cavity were measured using a 3D laser microscope. Then, the acoustic pressures and resonance frequencies of the pMUT and pMUT array were measured using a standard microphone (B&K 4954 A). The output acoustic pressure of the pMUT array at different driving voltages and distances was also measured. Moreover, the maximum output acoustic pressure at 3 cm above the array was recorded while the driving voltage was increased until the output pressure was saturated. Finally, a 3-axis motorized stage was used to move the microphone to measure the acoustic field created by the pMUT array.

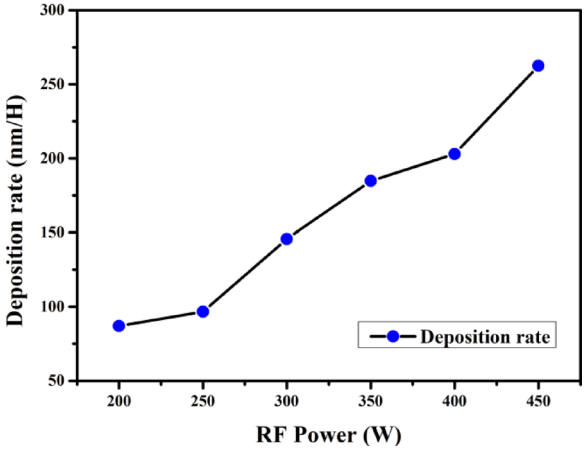

Fig. 6. Deposition rate of sputtered PZT without a sol-gel seed layer at different RF powers (250–450 W).

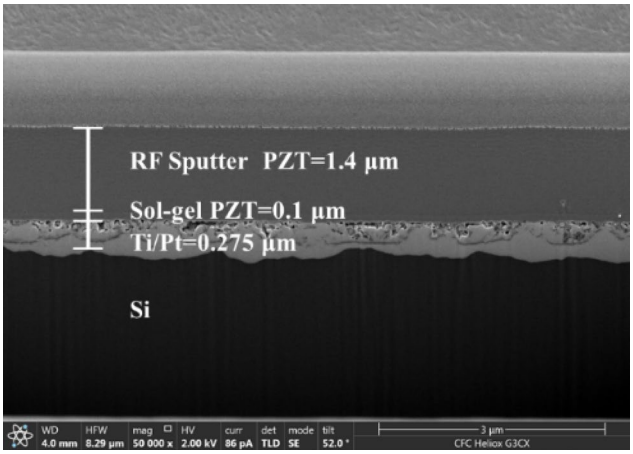

Fig. 7. FIB cross-sectional view of the PZT thin film made with the proposed method[23].

Result and discussion

Characterization of the PZT thin film

This study proposed a reliable fabrication method that grows PZT thin film using a custom RF sputter on top of a sol-gel PZT seed layer made by a commercial precursor. As Fig. 6 indicates, the deposition rate of sputtering the PZT thin film on Ti/Pt increased with the RF power, and the maximum deposition rate of 262.5 nm/h was achieved at 450 W RF power. Since the PZT target would be heated during the sputtering process due to ion bombardment, it might crack if the RF power was too high. Therefore, an RF power of 450 W was selected for the subsequent sputtering process to ensure reliability and a reasonable deposition rate. The uniformity of the sputtered PZT thin film was evaluated using a profile meter at five locations on the wafer. The average thickness and uniformity of the film sputtered using 450 W RF power for 7 h at 12 mTorr of Ar was 1.862 µm and 2.67%, respectively. After that, the sol-gel PZT layer was added before sputtering for 8 h using 450 W RF power to observe the deposition rate after adding the seed layer. Figure 7 shows the FIB cross-sectional image of the fabricated PZT thin film and the thickness of each layer[23]. The results indicated that using sol-gel PZT as a seed layer reduced the deposition rate from 262.5 nm/h to 175 nm/h because the seed layer had a lattice constant similar to the sputtered PZT more so than Ti/Pt did, resulting in a denser deposition. Furthermore, during the high-temperature annealing process, oxygen molecules leaked from the piezoelectric layer into the bottom electrode layer, causing oxidation and increasing the thickness of the titanium.

To optimize the annealing condition, this study annealed the PZT thin film using RTA at various temperatures: 600 °C, 650 °C, and 700 °C with a gradient of 30 °C/s for 180–300 s. Figure 8a,b are the optical microscopy (OM) images of the PZT thin films' surfaces with/without a sol-gel seed layer using the different annealing conditions. To provide a more detailed observation of the surface of the PZT thin films, scanning electron microscopy (SEM) images were taken in addition to OM images. Figure 8c,d display the SEM images of the PZT thin film grown without and with a seed layer after annealing at 700 °C for 300 s, respectively. It can be observed that the PZT thin films without a sol-gel seed layer exhibited numerous cracks after annealing and even delaminated from the substrate after annealing at 700 °C for 300 s. On the other hand, the films with a sol-gel seed layer

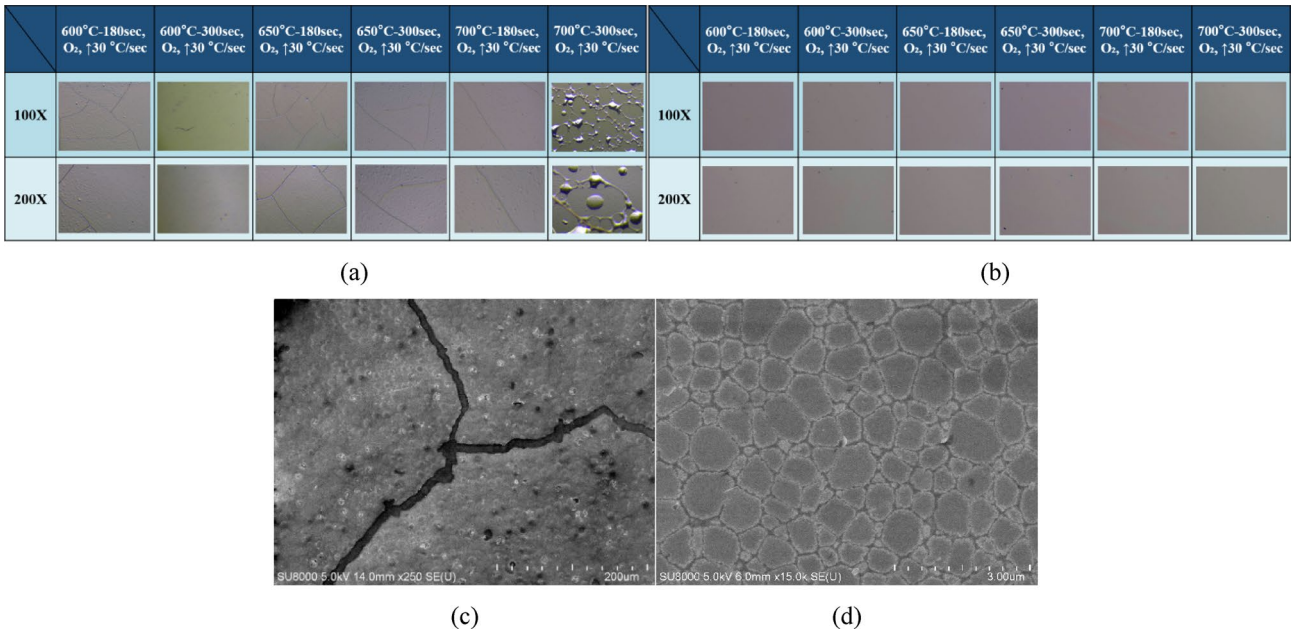

Fig. 8. Optical microscope images of RF-sputtered PZT at different annealing temperatures, (**a**) without a seed layer and (**b**) with a seed layer. SEM images of the PZT thin films grown (**c**) without and (**d**) with a seed layer.

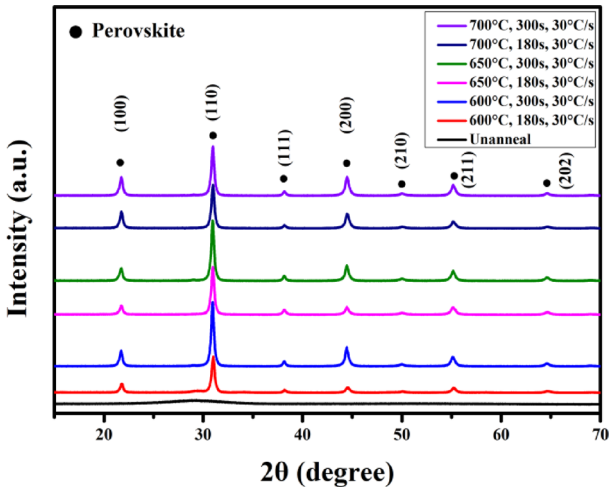

Fig. 9. XRD patterns of the proposed PZT thin film[23].

remained smooth and crack-free after annealing. Hence, the sol-gel seed layer effectively alleviated the thermal expansion mismatch between Pt and the sputtered PZT. As Fig. 9 shows, the X-ray diffraction pattern of the PZT thin films indicated that the piezoelectric thin film was amorphous after RF sputtering and transformed to the perovskite phase after annealing[23]. Therefore, high-temperature annealing facilitated the transformation of the PZT film into the perovskite phase, thereby enhancing the film's polarization. The dominant orientation of the proposed PZT thin film was PZT (110), one of the standard orientations of PZT that exhibit piezoelectric properties[30,31]. Besides, the thin film showed enhanced peak intensity in the (110) direction with increasing annealing time at each temperature.

The performance of the proposed PZT thin film deposition method was evaluated based on the remnant polarization value P_r and the transverse piezoelectric coefficient d_{31}. Figure 10a presents the P-E curves of a PZT thin film annealed at 600 °C for 300 s with different applied voltages, and Fig. 10b displays the P-E curves when 70 V was applied to the PZT thin films annealed at different temperatures. It could be observed that the P_r increased with the annealing temperatures. The PZT thin film annealed at 700 °C for 300 s resulted in a maximum P_r of 111.35 μC/cm² and a coercive electric field E_c of 211.6 kV/cm at 70 V[23]. As shown in Table 3[23], the proposed method had a remarkably high P_r value and coercive electric field compared to other published PZT

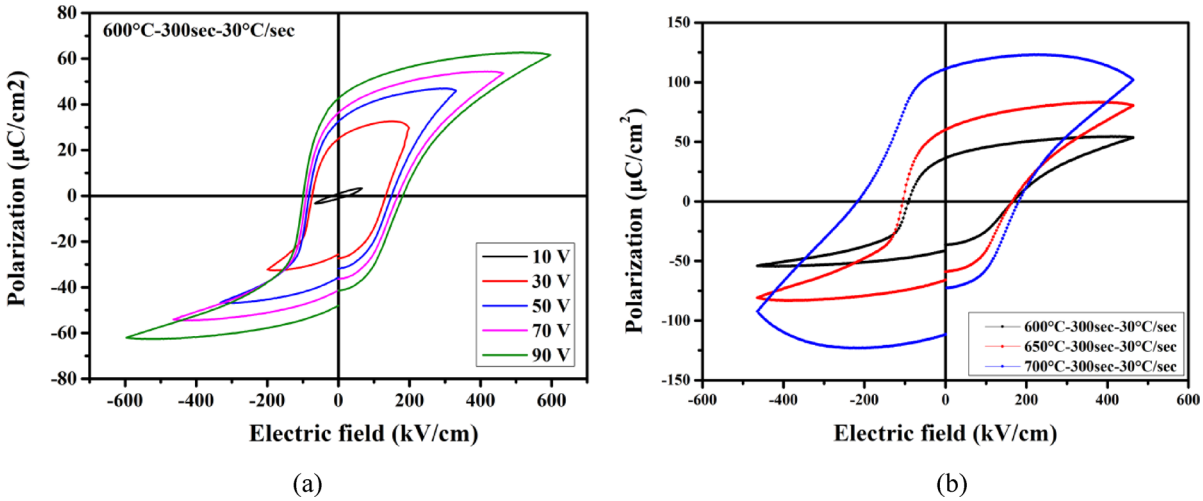

(a) (b)

Fig. 10. P-E curves of (**a**) the proposed PZT thin film annealed at 600 °C for 300 s with an applied voltage of 10 to 90 V, and (**b**) the proposed PZT thin film annealed at 600 °C, 650 °C and 700 °C for 300 s with an applied voltage of 70 V[23].

P_r (μC/cm²)	E_C (kV/cm)	Fabrication method	Remark	Reference
113.35	211.6	Sol-gel + RF sputter	Sol-gel PZT seed layer	This study
97	140	MOCVD	$SrTiO_3$/$SrRuO_3$ seed layer	[16]
65	72	Sol-gel	Nb doped PZT	[32]
50	150	Sol-gel	La doped PZT	[33]
37.78	79.14	RF sputter	-	[34]
26	33	RF sputter	-	[35]
56.8	51.1	Sol-gel and PLD	$PbTiO_3$ seed layer	[36]

Table 3. Comparison of the proposed PZT thin film with published PZT thin films[23].

thin films[17,32–36]. Besides, the transverse piezoelectric coefficient (d_{31}) of the proposed PZT thin film annealed at 650 °C for 300 s was calculated using Eq. (1) based on the measured dielectric constant (1145.60) at 70 V and positive remnant polarization (45 μC/cm²). The estimated d_{31} was 267.65 pm/V, which was close to previously reported results[25,30]. The proposed PZT thin film fabrication process using a thin sol-gel seed layer followed by a low-cost thicker sputtering PZT layer successfully resolved the issue of cracks caused by the thermal mismatch and showed excellent piezoelectric properties. Hence, the proposed method may be considered a cost-effective and reliable PZT thin film fabrication process for making piezoelectric sensors and actuators.

Characterization of the pMUTs and pMUT arrays

This study fabricated pMUTs and pMUT arrays to evaluate the potential of using the proposed PZT thin film in high sound pressure mid-air applications such as haptic feedback or acoustic levitation. Since 40 kHz is the most popular working frequency in current mid-air ultrasonic applications, this study designed the pMUT to operate at a resonance frequency of 40 kHz. To achieve an output frequency of 40 kHz, FEM simulations were conducted to optimize the design parameters. Figure 11 presents the simulation results of the relationship between the thickness of the piezoelectric layer and the center displacement when applying the DC voltage of 1 V. The maximum displacement of the center of the pMUT was obtained when the piezoelectric layer was 3 μm. Due to fabrication considerations, this study used 1.5 μm as the thickness of the PZT thin film. Figure 12 illustrates the simulated resonance frequencies corresponding to different radii. When the radius of the pMUT was about 700 μm, the resonance frequency was close to 40 kHz. Hence, this study fabricated pMUTs that measured from 600 μm to 775 μm in radius. Figure 12 also displays the measured resonance frequencies from five pMUTs with various radii, ranging from 52 kHz to 65 kHz. The measured and simulated resonance frequencies revealed a similar trend. However, the measured resonance frequencies consistently exceeded the calculated frequencies by roughly 10 kHz. Figure 13 shows the back etching profile of a 725 μm pMUT. The inner radius was 702.6 μm, and the outer radius was 716.3 μm. The difference between the designed and actual radius was less than 4%; thus, the resonance frequency was not influenced by the size errors. According to previous studies, the internal stress of the pMUT layer accumulated during the fabrication (usually between 20 MPa to 200 MPa) could affect the resonance frequency[37]. Hence, an internal stress of 70 MPa was added to the PZT layer of the COMSOL model. As Fig. 12 displays, the simulated resonance frequencies after adding an inner stress of 70 MPa matched

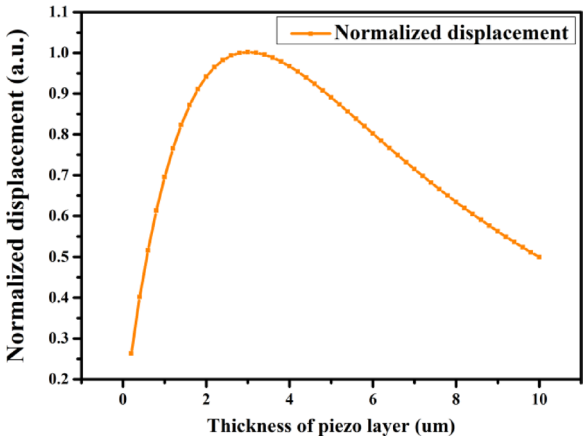

Fig. 11. Simulated center displacements of the pMUT versus the thickness of the PZT layer. The thickness of PZT ranged from 0.1 μm to 10 μm, and the pMUT was driven with 1 V DC voltage.

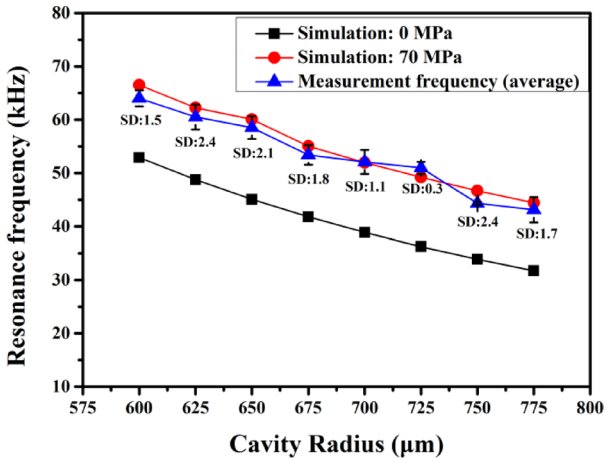

Fig. 12. Simulated and measured resonance frequencies of pMUTs. The black squares represent the resonance frequencies calculated by the FEM model without adding inner stress on the PZT layer. The red dots and blue triangles represent the simulated (with inner stress) and measured resonance frequencies, respectively.

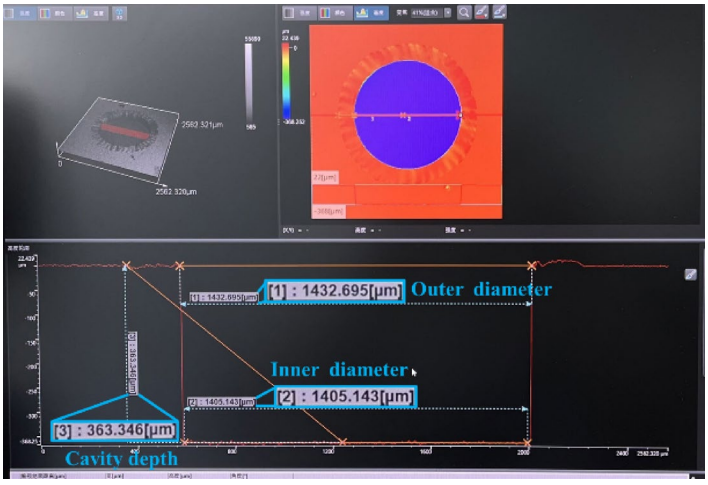

Fig. 13. Back etching profile of a 725 μm pMUT.

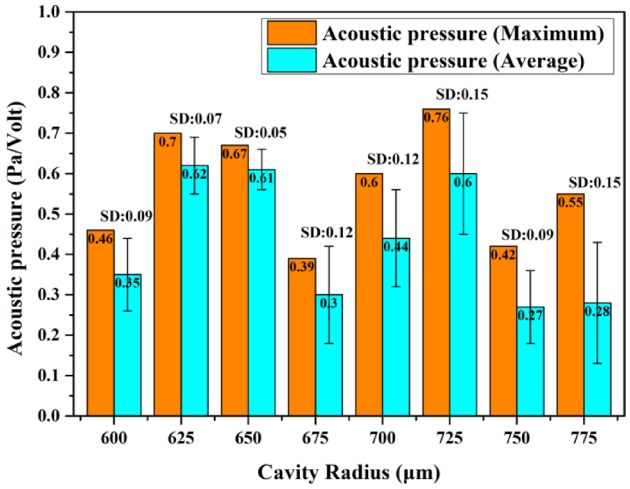

Fig. 14. Acoustic pressure of the proposed PMUT with various cavity radii, measured at 3 cm above, with a driving voltage of 10 V_{PP} at the resonance frequency[23].

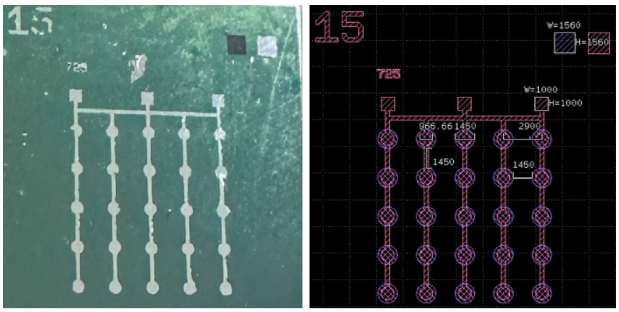

Fig. 15. (**a**) Picture and (**b**) layout of the 725 μm pMUT array with geometric parameters. The pitch and size of the pMUT array are 1450 μm and 1.7 cm^2, respectively.

the measured results, which explained the observed difference between the simulated and measured resonance frequencies.

As mentioned in *Fabrication and characterization of pMUTs and pMUTs array*, the acoustic output pressure of pMUTs and pMUT array was measured to evaluate the capability of the proposed PZT thin film for further applications. Figure 14 presents the acoustic output pressure measured by a standard microphone at 3 cm above the pMUTs with cavity radii ranging from 600 μm to 775 μm[23]. Each pMUT was driven by a 10 V_{PP} burst signal with 100 cycles during the measurement. These results indicated that the maximum output acoustic pressure efficiency (0.764 Pa/V) was measured at the frequency of 52.2 kHz for the pMUT with a radius of 725 μm. Hence, the 5 × 5 pMUT array was fabricated based on the 725 μm pMUT with a 1450 μm pitch (Fig. 15). During the measurements, the array was driven at 52.2 kHz with varying applied voltage, and the sound pressure was measured at different distances above the center of the array. As Fig. 16 displays, the acoustic pressure efficiency was 6.912 Pa/V at 1 cm above the array when the input signal was 12.5 V_{PP}. In addition, the acoustic pressure of each pMUT was measured at 3 cm above the array with a driving voltage of 12.5 V_{PP}, as shown in Fig. 17. The average acoustic pressure of the entire array was 2.85 Pa, which was used in the k-Wave simulation. Figure 18a shows the simulated acoustic pressure distribution at 3 cm above the array, indicating a maximum acoustic pressure of approximately 33 Pa, while Fig. 18b shows the measured acoustic pressure distribution, indicating a maximum acoustic pressure of 29.6 Pa. Although the measured peak acoustic pressure was similar to the simulation, asymmetry was observed in the acoustic field distribution. This can be attributed to the unevenness in the output acoustic pressure of each element in the array, as shown in Fig. 17. Besides, the pressure distribution when focusing the acoustic waves 3 cm above the pMUT array was also evaluated, as shown in Fig. 18c. The peak output acoustic pressure was 1.5 times larger than the unfocused situation and reached 50.5 Pa. To produce a higher acoustic pressure from the array, the driving voltage was increased to 50 V_{PP}, and the microphone readings showed that the acoustic output pressure of the array reached 87.4 Pa at 3 cm above its center. Table 4 compares the published air-coupled PZT-based pMUTs with this work[38–40]. Among known devices, ours had a relatively high total output acoustic pressure and better transmission efficiency at sub-100 kHz. Considering the small size of the array itself and the favorable performance of the fabricated thin film, this configuration

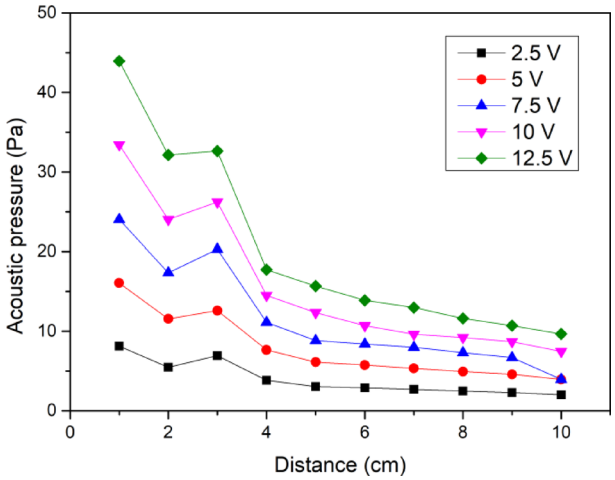

Fig. 16. Acoustic pressures of the pMUT array measured from 3 cm above the center with different driving voltages at 52.2 kHz.

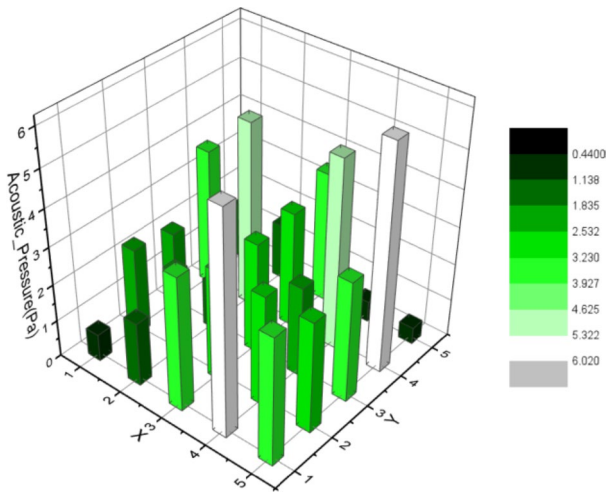

Fig. 17. Output acoustic pressure of pMUT on the 725 μm pMUT array driving at 52.2 kHz with 12.5 V_{PP} driven voltage.

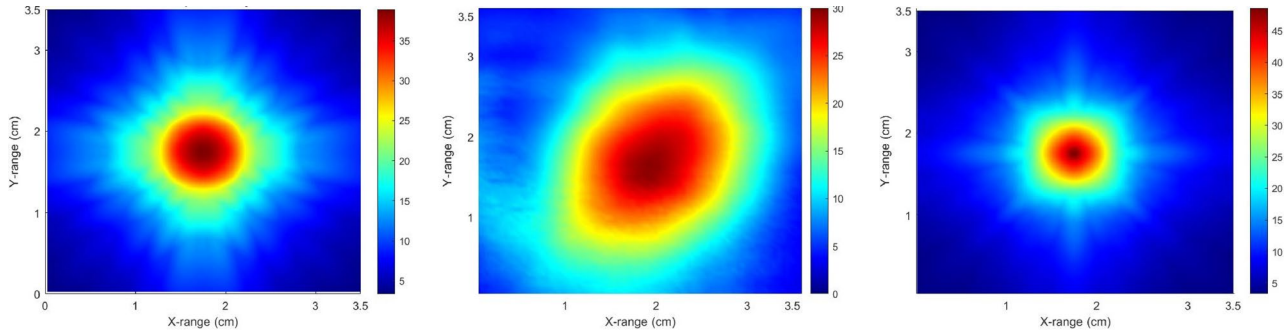

Fig. 18. (**a**) Simulated and (**b**) measured acoustic pressure distributions of the unfocused 725 μm radius pMUT array. (**c**) Simulated acoustic pressure distributions of the focused 725 μm radius pMUT array.

	This study	[38]	[39]	[40]
Acoustic pressure (Pa)	87.4	2.07	4.42	0.43
Material of actuation layer	PZT	PZT	PZT	PZT/ Polycarbonate (PC)
PMUT radius (μm)	725	625	725	6000
Array size	5 × 5	2 × 2	1 × 1	Five-spot pattern
Operating frequency (kHz)	52.2	46	40.48	21.75
Measured distance (cm)	3	33	3	20
Drive voltage (V_{PP})	50	5	50	10
Transmission efficiency (Pa/V)	1.748	0.414	0.088	0.043
Transmission efficiency per area (Pa/V/cm^2)	1.299	4.6	5.353	0.038

Table 4. Comparison of the proposed pMUT array with published air-coupled pMUTs.

will decrease the complexity of the pMUT layout and circuit design for controlling the pMUTs individually when acoustic beamforming is required. Hence, the proposed PZT thin film fabrication method is promising for making pMUTs used in high acoustic pressure mid-air ultrasonic applications.

Conclusion

This study demonstrated a fabrication method for PZT thin films using RF sputtering on top of a sol-gel PZT seed layer. The deposition rate of the sputtered PZT thin film was found to increase with RF power, with the maximum deposition rate achieved at 450 W RF power. The use of a sol-gel PZT seed layer resulted in a reduction in the deposition rate but solved the film cracking issue caused by thermal expansion mismatch. High-temperature annealing facilitated the transformation of the PZT film into the perovskite phase, enhancing its polarization characteristics.

After comparing with previous research, this study successfully demonstrated a PZT thin film with better remanent polarization results using a concise fabrication method without doping rare metals or depositing conductive metal oxides. The proposed method resulted in a maximum P_r of 111.35 μC/cm² and a coercive electric field E_c of 211.6 kV/cm at 70 V, supporting its use in high-performance applications. The proposed pMUT devices could be applied in various potential applications, including fingerprint recognition, distance measurement, and ultrasonic haptic feedback, such as non-contact human-machine interfaces and interactive displays. Due to some technical restrictions, the structure of the pMUTs array was designed in series, which prevents actual beam focusing. Therefore, evaluating the output acoustic pressure becomes essential in this study. The fabricated 5 × 5 pMUTs array was driven at the response frequency of 52.5 kHz and the driving voltage of 50 V_{PP}, and the acoustic pressure output reached 87.4 Pa at 3 cm above the center of the array. The entire fabrication only required standard types of equipment for RF sputtering, spin coating, and RTA. Besides, the PZT target and sol-gel solution were both accessible commercial products. Therefore, the proposed method was reliable and easy to reproduce, which fulfills the requirements of making piezoelectric micro-electromechanical system devices.

Data availability

The authors confirm that the data supporting the findings of this study are available within the article.

Received: 20 February 2025; Accepted: 25 September 2025
Published online: 31 October 2025

References

1. Mo, J. H., Robinson, A., Fitting, D., Terry, F. & Carson, P. *Proceedings., IEEE Ultrasonics Symposium*. 801–804. https://doi.org/10.1109/ULTSYM.1989.67097 (IEEE, 1989).
2. Birjis, Y. et al. Piezoelectric micromachined ultrasonic transducers (PMUTs): performance metrics, advancements, and applications. *Sensors* **22**, 9151. https://doi.org/10.3390/s22239151 (2022).
3. Drinkwater, B. W. & Wilcox, P. D. Ultrasonic arrays for non-destructive evaluation: A review. *NDT E Int.* **39**, 525–541. https://doi.org/10.1016/j.ndteint.2006.03.006 (2006).
4. Jiang, X. et al. Ultrasonic fingerprint sensor with transmit beamforming based on a PMUT array bonded to CMOS circuitry. *IEEE Trans. Ultrason. Ferroelectr. Freq. Control.* **64**, 1401–1408. https://doi.org/10.1109/TUFFC.2017.2703606 (2017).
5. Dausch, D. E. et al. In vivo real-time 3-D intracardiac echo using PMUT arrays. *IEEE Trans. Ultrason. Ferroelectr. Freq. Control.* **61**, 1754–1764. https://doi.org/10.1109/TUFFC.2014.006452 (2014).
6. Przybyla, R. J. et al. In-air rangefinding with an AlN piezoelectric micromachined ultrasound transducer. *IEEE Sens. J.* **11**, 2690–2697. https://doi.org/10.1109/JSEN.2011.2157490 (2011).
7. Halbach, A. et al. *20th International Conference on Solid-State Sensors, Actuators and Microsystems & Eurosensors XXXIII (TRANSDUCERS & EUROSENSORS XXXIII)*. 158–161. https://doi.org/10.1109/TRANSDUCERS.2019.8808775 (IEEE, 2019).
8. Atif, R. et al. Solution blow spinning of polyvinylidene fluoride based fibers for energy harvesting applications: A review. *Polymers* **12**, 1304. https://doi.org/10.3390/polym12061304 (2020).
9. Fraga, M. A., Furlan, H., Pessoa, R. & Massi, M. Wide bandgap semiconductor thin films for piezoelectric and piezoresistive MEMS sensors applied at high temperatures: an overview. *Microsyst. Technol.* **20**, 9–21. https://doi.org/10.1007/s00542-013-2029-z (2014).

10. Vacca, M. et al. Electric clock for nanomagnet logic circuits. *Field Coup. Nanocomput. Parad. Progr. Perspect.* 73–110. https://doi.org/10.1007/978-3-662-43722-3_5 (2014).
11. Velu, G. & Remiens, D. Electrical properties of sputtered PZT films on stabilized platinum electrode. *J. Eur. Ceram. Soc.* **19**, 2005–2013. https://doi.org/10.1016/S0955-2219(99)00008-4 (1999).
12. Hu, H., Peng, C. & Krupanidhi, S. Effect of heating rate on the crystallization behavior of amorphous PZT thin films. *Thin Solid Films*. **223**, 327–333. https://doi.org/10.1016/0040-6090(93)90540-6 (1993).
13. Oikawa, T., Aratani, M., Funakubo, H., Saito, K. & Mizuhira, M. Composition and orientation dependence of electrical properties of epitaxial Pb (Zr x Ti 1 – x) O 3 thin films grown using metalorganic chemical vapor deposition. *J. Appl. Phys.* **95**, 3111–3115. https://doi.org/10.1063/1.1645646 (2004).
14. Dai, C. L. et al. Thermal effects in PZT: diffusion of titanium and recrystallization of platinum. *Mater. Sci. Engineering: A*. **384**, 57–63. https://doi.org/10.1016/j.msea.2004.05.067 (2004).
15. Di, X. & Muralt, P. *2017 Joint IEEE International Symposium on the Applications of Ferroelectric (ISAF)/International Workshop on Acoustic Transduction Materials and Devices (IWATMD)/Piezoresponse Force Microscopy (PFM)*. 33–36. https://doi.org/10.1109/ISAF.2017.8000205 (IEEE, 2017).
16. Morioka, H., Asano, G., Oikawa, T., Funakubo, H. & Saito, K. Large remanent polarization of 100% polar-axis-oriented epitaxial tetragonal Pb (Zr0. 35Ti0. 65) O3 thin films. *Appl. Phys. Lett.* **82**, 4761–4763. https://doi.org/10.1063/1.1586993 (2003).
17. Abe, K., Tomita, H., Toyoda, H., Imai, M. I. M. & Yokote, Y. Y. Y. PZT thin film Preparation on Pt-Ti electrode by RF sputtering. *Jpn. J. Appl. Phys.* **30**, 2152. https://doi.org/10.1143/JJAP.30.2152 (1991).
18. Nguyen, M. D. et al. Highly oriented growth of piezoelectric thin films on silicon using two-dimensional nanosheets as growth template layer. *ACS Appl. Mater. Interfaces* **8** 31120–31127. https://doi.org/10.1021/acsami.6b09470 (2016).
19. Chu, S. Y., Chen, T. Y., Tsai, I. T. & Water, W. Doping effects of Nb additives on the piezoelectric and dielectric properties of PZT ceramics and its application on SAW device. *Sens. Actuators A: Phys.* **113**, 198–203. https://doi.org/10.1016/j.sna.2004.02.020 (2004).
20. Zhang, Q. & Whatmore, R. Improved ferroelectric and pyroelectric properties in Mn-doped lead zirconate titanate thin films. *J. Appl. Phys.* **94**, 5228–5233. https://doi.org/10.1063/1.1613370 (2003).
21. Nordseth, Ø., Tybell, T., Grepstad, J. & Epitaxial Pb, La)(Zr, Ti) O3 thin films on buffered Si (100) by on-axis radio frequency Magnetron sputtering. *Thin Solid Films*. **517**, 2623–2626. https://doi.org/10.1016/j.tsf.2008.10.038 (2009).
22. Sanchez, L. M. et al. Optimization of PbTiO3 seed layers and Pt metallization for PZT-based piezomems actuators. *J. Mater. Res.* **28**, 1920–1931. https://doi.org/10.1557/jmr.2013.172 (2013).
23. Kao, C. L. et al. *2023 IEEE International Ultrasonics Symposium (IUS)*. 1–4. https://doi.org/10.1109/IUS51837.2023.10308299 (IEEE, 2023).
24. Chun, D. M., Sato, M. & Kanno, I. Precise measurement of the transverse piezoelectric coefficient for thin films on anisotropic substrate. *J. Appl. Phys.* **113** https://doi.org/10.1063/1.4789347 (2013).
25. Le Rhun, G. et al. *20th International Conference on Solid-State Sensors, Actuators and Microsystems & Eurosensors XXXIII (TRANSDUCERS & EUROSENSORS XXXIII)*. 1800–1802. https://doi.org/10.1109/TRANSDUCERS.2019.8808241 (IEEE, 2019).
26. Udayakumar, K. et al. *[1991] Proceedings. IEEE Micro Electro Mechanical Systems*. 109–113. https://doi.org/10.1109/MEMSYS.1991.114779 (IEEE, 1991).
27. Jeong, Y. et al. Fully flexible PMUT based on polymer materials and stress compensation by adaptive frequency driving. *J. Microelectromech. Syst.* **30**, 137–143. https://doi.org/10.1109/JMEMS.2020.3043052 (2020).
28. Hoshi, T., Iwamoto, T. & Shinoda, H. *World Haptics 2009-Third Joint EuroHaptics Conference and Symposium on Haptic Interfaces for Virtual Environment and Teleoperator Systems*. 256–260. https://doi.org/10.1109/WHC.2009.4810900 (IEEE, 2009).
29. Wang, H., Godara, M., Chen, Z. & Xie, H. A one-step residue-free wet etching process of ceramic PZT for piezoelectric transducers. *Sens. Actuators A: Phys.* **290**, 130–136. https://doi.org/10.1016/j.sna.2019.03.028 (2019).
30. Cueff, M. et al. *IEEE International Ultrasonics Symposium*. 1948–1951. https://doi.org/10.1109/ULTSYM.2011.0485 (IEEE, 2011).
31. Ambika, D., Kumar, V., Imai, H. & Kanno, I. Sol-gel deposition and piezoelectric properties of {110}-oriented Pb (Zr0. 52Ti0. 48) O3 thin films. *Appl. Phys. Lett.* **96**, https://doi.org/10.1063/1.3293446 (2010).
32. Li, J. F., Zhu, Z. X. & Lai, F. P. Thickness-dependent phase transition and piezoelectric response in textured Nb-doped Pb (Zr0. 52Ti0. 48) O3 thin films. *J. Phys. Chem. C.* **114**, 17796–17801. https://doi.org/10.1021/jp106384e (2010).
33. Shannigrahi, S. & Jang, H. M. Fatigue-free lead zirconate titanate-based capacitors for nonvolatile memories. *Appl. Phys. Lett.* **79**, 1051–1053. https://doi.org/10.1063/1.1392970 (2001).
34. Bi, Z., Zhang, Z. & Fan, P. *Journal of Physics: Conference Series*. **120**. https://doi.org/10.1088/1742-6596/61/1/025 (IOP Publishing, 2007).
35. Wilke, R. H. et al. Sputter deposition of PZT piezoelectric films on thin glass substrates for adjustable x-ray optics. *Appl. Opt.* **52**, 3412–3419. https://doi.org/10.1364/AO.52.003412 (2013).
36. Pandey, S., James, A., Prakash, C., Goel, T. & Zimik, K. Electrical properties of PZT thin films grown by sol–gel and PLD using a seed layer. *Mater. Sci. Engineering: B*. **112**, 96–100. https://doi.org/10.1016/j.mseb.2004.06.011 (2004).
37. Akhbari, S. et al. *28th IEEE International Conference on Micro Electro Mechanical Systems (MEMS)*. 837–840. https://doi.org/10.1109/MEMSYS.2015.7051089 (IEEE, 2015).
38. Luo, G. L., Kusano, Y. & Horsley, D. A. Airborne piezoelectric micromachined ultrasonic transducers for long-range detection. *J. Microelectromech. Syst.* **30**, 81–89. https://doi.org/10.1109/JMEMS.2020.3037298 (2020).
39. Liu, Y. H. et al. Development of an Air-Coupled piezoelectric micromachined ultrasonic transducer using Sol-Gel PZT thin film for Fast-Prototyping. *IEEE Open. J. Ultrason. Ferroelectr. Freq. Control.* **4**, 27–36. https://doi.org/10.1109/OJUFFC.2024.3397630 (2024).
40. Casset, F. et al. *25th International Conference on Thermal, Mechanical and Multi-Physics Simulation and Experiments in Microelectronics and Microsystems (EuroSimE)*. 1–4. https://doi.org/10.1109/EuroSimE60745.2024.10491429 (IEEE, 2024).

Acknowledgements

This work was supported in part by the National Science and Technology Council (NSTC) under NSTC 114-2313-B-006-010. The authors also gratefully acknowledge the use of XRD001900 of 109-2923-E-006-002-MY3 belonging to the Core Facility Center of National Cheng Kung University.

Author contributions

JLL, YHL, CLK, and CHH participated in writing - original draft, writing - review & editing, methodology, formal analysis, data curation, conceptualization. SWW, HJH, HCL, CYL participated in validation, investigation, formal analysis. CYC participated in software, investigation, formal analysis. YHW and CHH participated in project administration. All authors have read and approved the final manuscript.

Declarations

Competing interests
The authors declare no competing interests.

Additional information
Correspondence and requests for materials should be addressed to Y.-H.W. or C.-H.H.

Reprints and permissions information is available at www.nature.com/reprints.

Publisher's note Springer Nature remains neutral with regard to jurisdictional claims in published maps and institutional affiliations.